Assessment of Ionospheric Impact on LAAS Using WAAS Supertruth Data

Ming Luo, Sam Pullen, Dennis Akos, Gang Xie, Seebany Datta-Barua, Todd Walter, and Per Enge
Stanford University

ABSTRACT

In order to reflect the impact of spatial ionospheric gradients on Local Area Augmentation System (LAAS) users, the LAAS Ground Facility (LGF) broadcasts a conservative standard deviation ($\sigma_{vert\_iono\_gradient}$ or σ_{vig}) for these errors that is included in the calculation of protection levels (bounds on user position errors). However, "supertruth" data provided by the Wide Area Augmentation System (WAAS) for a severe ionospheric storm in 2000 provided an example of a sudden, sharp change in ionospheric delays that implied a spatial gradient far larger than what is typical, even during these storms. It is impractical for LAAS to increase $\sigma_{vert\_iono\_gradient}$ to bound these rare events; thus they must be classified as failures to be detected and alerted by the LGF before the user integrity risk increases to an unacceptable level.

The goal of this study is to assess the integrity risk to LAAS users posed by these sharp ionosphere gradients and to determine if additional protection is needed for LAAS users. The anomaly observed in the supertruth data has been modeled as a sharp "wave front" in which a specified linear change in vertical ionosphere delay occurs over a specified horizontal distance. This wave front is assumed to move at a constant horizontal speed and direction relative to the ground. Each of these parameters can be varied to assess the sensitivity of LAAS to a wide variety of ionospheric spatial anomalies.

By simulating ionosphere wave fronts at both aircraft and LAAS Ground Facility (LGF), we have studied the resulting differential errors. We have also tested how quickly the anomaly can be detected by the Stanford LGF prototype known as the Integrity Monitor Testbed (IMT). In the scenarios examined thus far, the IMT carrier-phase measurement quality alerts within 1 – 2 seconds of the wave front crossing an IMT Ionospheric Pierce Point (IPP), whereas smaller (less hazardous) gradients are detected within several minutes by the code-carrier divergence monitor. The scenario of most concern is when the wave front "comes up from behind" an aircraft approaching a LAAS-equipped airport and overtakes one or more aircraft pierce points several minutes before the aircraft reaches the runway threshold. In this case, the differential error growth is not cut off by IMT detection because the wave front has not yet crossed an IMT pierce point.

We have examined many variations of the basic ionosphere wave front anomaly scenario in the range domain and the position domain. Based on the results to date, we believe that only a "multiple-worst-case" combination of gradient size, depth, direction of travel, approach speed, and phasing with the aircraft approach leads to any appreciable user hazard. Because of the rarity of this combination of circumstances, the integrity threat posed by ionosphere wave fronts appears to be acceptably small for Category I precision approaches. However, we are not confident that this is the case for Category II/III approaches and landings. We are continuing to assess wave-front variations and LAAS impacts to further validate this conclusion.

1.0 INTRODUCTION

The ionosphere is a dispersive medium located in the region of the upper atmosphere between about 50 km to about 1000 km above the earth [1]. The radiation of the sun produces free electrons and ions that cause phase advance and group delay to radio waves. As GPS signals traverse the ionosphere, they are delayed by an amount proportional to the number of total electron content. The state of the ionosphere is a function of intensity of the solar activity, magnetic latitude, local time, and other factors. The error introduced by the ionosphere into the GPS signal is highly variable and difficult to model.

WAAS continuously processes ionospheric measurements for the region around the Conterminous United States (CONUS) as obtained from its network of twenty-five dual-frequency ground stations. This data is enhanced in post-processing by removing satellite and ground station inter-frequency biases to create “supertruth” data. A snapshot of an ionospheric anomaly observed from WAAS supertruth data on April 6, 2000, is shown in Figure 1. The vertical and horizontal axes denote latitude and longitude, in degrees, with positive values north of the equator and east of the prime meridian. The WAAS station ZDC (near Washington D.C.) is located at 39° N, 77.5° W. Superimposed on the outline of the U.S. is a color map that indicates contours of estimated vertical ionospheric delay. The gradient observed at the IPPs between ZDC and SVN 40 appears in sharp definition,

separating the light green from the dark blue areas right near the pierce points. In addition it seems this gradient may be part of a larger structure, a front whose wall runs roughly East-West. The detailed description on how to extract the iono information from WAAS raw data can be found in [2].

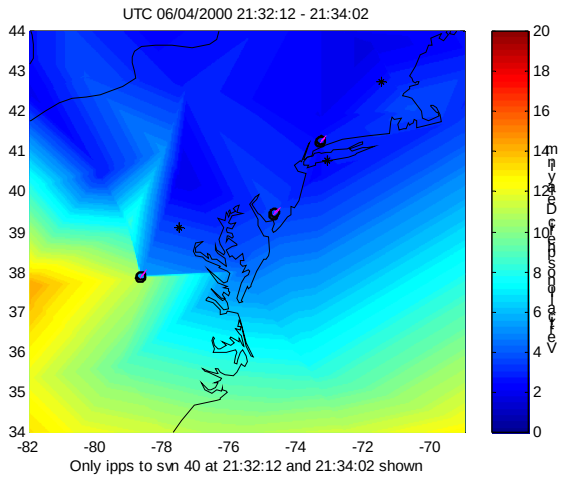

Figure 1: WAAS Supertruth Ionosphere Data (Anomaly of April 6-7, 2000)

Based on the WAAS supertruth data, the iono anomaly can be modeled as a semi-infinite "cloud" with a front. For the anomaly observed in Figure 1, the iono front was moving at about 110 m/s. The maximum vertical iono delay was about 6 meters over a gradient of about 19 km thick at the IPP (assumed to be at a 350-km altitude). A linear ramp was assumed for the transition area between the nominal iono region and the maximum iono region. Figure 2 illustrates this model.

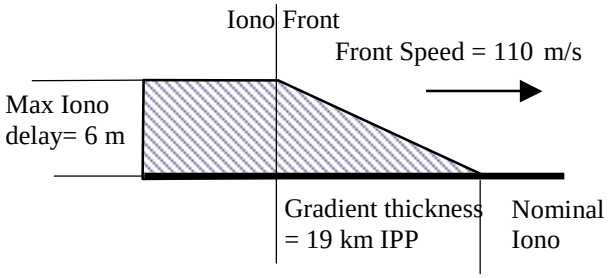

Figure 2: Simplified Model of Ionosphere Anomaly

We are interested in the impact of this type of anomaly on LAAS users. If both the user and the LAAS LGF see the same ionospheric delay, then there is no impact since the user error induced by the ionosphere will cancel out when the differential corrections broadcast by the LGF are applied. However, if the user and the LGF see different ionosphere delays, then there will be some differential error. In particular, if for a particular LAAS airport and GPS satellite geometry, the user is "hit" by the ionosphere wave front before the LGF is, there is a window where no ionosphere correction is available to the user. A "near-worst-case" scenario of this sort is sketched in Figure 3. In this scenario, the user is 45 km away (the limit of LAAS VHF data broadcast coverage [5]) and is approaching the LGF at a speed of 70 m/s. The ionosphere front is behind the airplane and is moving in the same direction at a speed of 110 m/s. The ionosphere front is going to "catch" the airplane, pass it, and eventually hit the IPP between the LGF and the satellite. The LGF "sees" the ionosphere from then on and gradually incorporates it into its differential corrections.

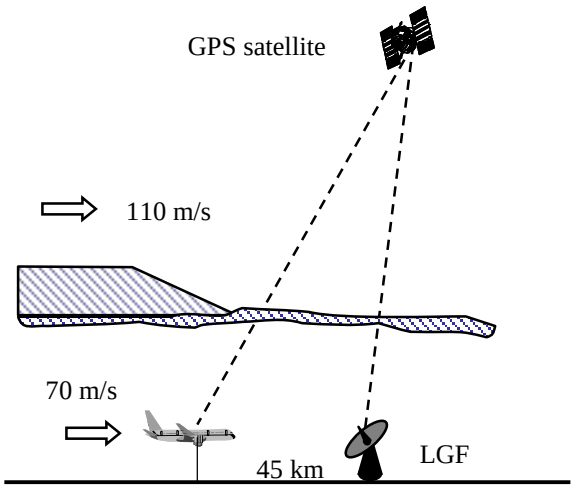

Figure 3: A "Near-Worst-Case" LAAS User Scenario

2.0 RANGE DOMAIN ANALYSIS

In the scenario illustrated in Figure 3, the range-domain differential error that the user observes builds up as the error enters its carrier-smoothing filter:

$$PR_s(k) = \frac{1}{N_s} PR(k) + \frac{N_s - 1}{N_s}[PR_s(k-1) + \phi(k) - \phi(k-1)] \quad (1)$$

where:

$PR_s(k)$ – Carrier Smoothed Code (CSC) at k^{th} epoch.

$PR(k)$ – raw pseudorange measurement at k^{th} epoch.

N_s – Smoothing filter time constant (200 epochs, or 100 seconds)

$\phi(k)$ – carrier phase at k^{th} epoch.

Both the airborne user and the LGF apply first-order carrier smoothing using (1) with the same smoothing time constant.

The ionosphere impact on the user and the LGF are shown in Figure 4. The x-axis is the time step during the airplane approach, measured in epochs with a 2 Hz update rate. The blue curve shows the ionosphere-induced error on the user's CSC. At time zero of the simulation, the iono front is just about to touch the airplane, and the ionosphere-induced error is zero. Since the iono delays pseudorange and advances carrier phase measurements, when the user starts to see the gradient, the impact on carrier phase dominates; thus the resulting error is negative. After a couple of time constants pass, the impact on raw pseudorange starts to dominate, and the resulting error grows in the positive direction. The simulation ends when the airplane lands (at epoch 1286) before the error approaches the constant state, which is the maximum ionosphere gradient of 6 meters.

The red line in Figure 4 shows the ionosphere-induced error in LGF CSC. At epoch 818, the LGF is hit by the ionosphere front, and the error curve takes about the same shape as the user – has a negative dip at the beginning, grows positively after about 2τ, and approaches the maximum error of 6 meters. The green dashed curve shows the resulting user differential error, which is simply the difference between the blue and the red curves. Note that the differential user error becomes greater when LGF first sees the ionosphere front before the correction helps on reducing the error at later stage. Under this scenario, the maximum differential error reaches 5.2 meters.

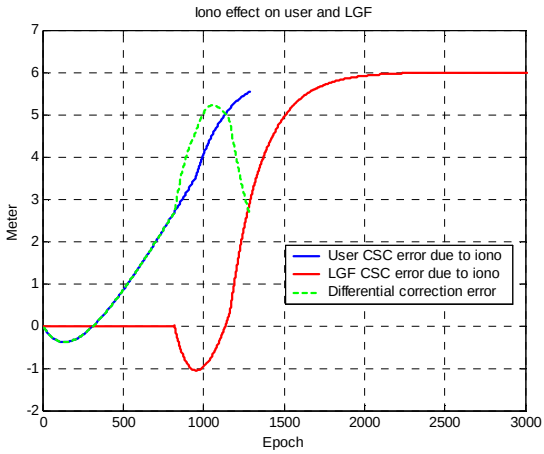

Figure 4: Ionosphere Gradient Impact (Range Error)

2.1 LGF Detection Capability

Given the model shown in Figure 2, the LGF will be impacted by the ionosphere front at some point during an approach. Once it is affected, one or more of the existing LGF integrity monitors may issue an alert despite not being designed specifically to detect this anomaly. In order to quantify this, we used the Integrity Monitor Testbed (IMT), a LAAS LGF prototype developed at Stanford University, to simulate the detection ability of the LGF. The IMT consists of various monitors to address integrity concerns such as satellite signal failures, ephemeris anomalies, receiver problems, RF interference, etc. Though each monitor was designed to target different failure modes, we found that the multiple monitors of the IMT are sensitive to more than one type of anomaly, and several of them can detect the ionosphere spatial gradient modeled here. A quick description of those monitors is given in this section. More detailed descriptions and algorithms can be found in [6,7].

MQM (*Measurement Quality Monitoring*): This function is designed to detect sudden jumps or rapid acceleration in pseudorange and carrier phase measurements. Before carrier smoothing occurs on each epoch, the last 10 epochs (5 seconds) of carrier phase measurements of all ranging sources being tracked are used to fit the following 2nd-order model:

$$\phi^* = \phi_0^* + \frac{d\phi^*}{dt}\Delta t + \frac{d^2\phi^*}{dt^2}\frac{\Delta t^2}{2}; \qquad (2)$$

where:

$$\phi^* = \phi - \phi^{corr} - \phi^{ave} = \hat{\phi} - \phi^{ave}\ ; \qquad (3)$$

$$\phi^{ave} = \frac{1}{N_c}\sum_{i=1}^{N_c}\phi_i\ ; \qquad (4)$$

$$\phi^{corr} = R^{SV} + \tau^{SV}; \qquad (5)$$

and where N_c is the number of satellites in the "common set" across the three IMT reference receivers, and R^{SV} and τ^{SV} are the user-to-satellite range and satellite clock corrections, respectively. Three test statistics are defined:

$$Step\,test \equiv \phi^*_{meas} - \phi^*_{pred}; \qquad (6)$$

$$Ramp\ \ test \equiv \frac{d\phi^*}{dt} \qquad (7)$$

$$Acceleration\ test \equiv \frac{d^2\phi^*}{dt^2}; \qquad (8)$$

where ϕ^*_{meas} is the computed value of ϕ^* at the current epoch, and ϕ^*_{pred} is the value computed from (2) based on the coefficients ϕ_0^*, $\frac{d\phi^*}{dt}$, and $\frac{d^2\phi^*}{dt^2}$ computed from a least-squares fit to the last 10 phase measurements.

After smoothing is completed on a given epoch, the MQM innovation test statistic is computed to detect unusual pseudorange deviations:

$$Inno(k) \equiv PR(k) - \left(PR_S(k-1) + \phi(k) - \phi(k-1)\right) \qquad (9)$$

SQM (Signal Quality Monitor) code-carrier divergence: This function was designed to address potential satellite failures that cause code-carrier divergence but will also detect unusual divergence due to the ionosphere. The raw observable code-minus-carrier (denoted as z) is fed into a time-varying filter:

$$d_k = \frac{\tau_d(k) - T}{\tau_d(k)} d_{k-1} + \frac{1}{\tau_d(k)} (z_k - z_{k-1}) \quad (10)$$

$$\text{where} \quad \tau_d(k) = \begin{cases} kT, & kT < \tau_{d\max} \\ \tau_{d\max}, & kT \geq \tau_{d\max} \end{cases}$$

The simulation of the baseline model of the ionosphere anomaly was conducted within the IMT to determine the time needed to detect it. The results are illustrated in Figure 5 and are summarized in Table 1.

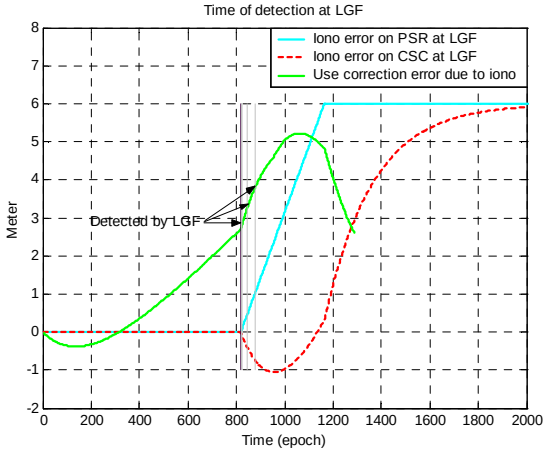

Figure 5: LGF Detection of Ionosphere Anomaly

IMT Monitor	MQM innova -tion	MQM Acc	MQM Ramp	SQM code-carrier divergence
Time-to-detect (second)	76	1.5	2	31

Table 1: IMT Time-to-Alert Summary

Among the multiple monitors that can detect this anomaly, MQM Acceleration and Ramp respond fastest: 1.5 and 2 seconds respectively. When IMT flags such an anomaly, the affected measurement is excluded, and anomaly-induced error is no longer present. In this case, LGF prompt detection reduces the maximum differential range error from 5.2 meters to about 2.7 meters.

2.2 Sensitivity to Model Parameters

The results shown thus far are based on the parameters of the baseline model (Figure 2) only. In order to examine the sensitivity to the model parameters and to examine the robustness of LGF detection, we expanded each variable to certain range started from their base-line-case values. We keep all the other parameters at their baseline value and only vary the one parameter each time.

The ionosphere anomaly shown in Figure 1 is huge. A 6-meter gradient over only 19 km is far higher than typical one-sigma gradients of 1 – 5 mm/km [8]. When anomalies like this occur during ionosphere storms, the actual gradient will be of varying amplitude. Differential user error during an approach is plotted with different maximum vertical gradient amplitudes in Figure 6. The thick black line is for the baseline situation (6-meter amplitude). As expected, differential error is directly proportional to the vertical ionosphere gradient amplitude.

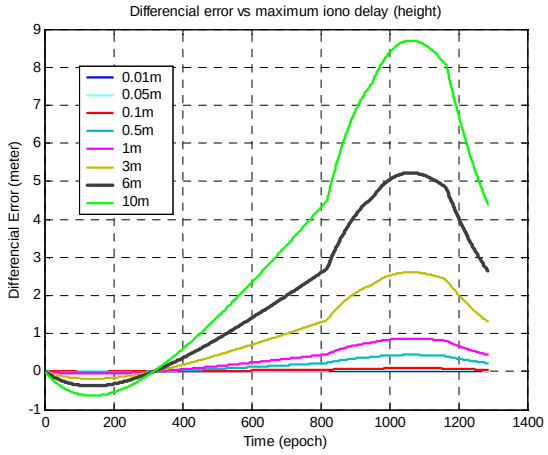

Figure 6: Differential Error Sensitivity to Ionosphere Gradient Amplitude

The maximum differential error over time during an approach is plotted as a function of ionosphere gradient amplitude in Figure 7. The impact of LGF detection is also shown on the plot. Since the threshold of the MQM Ramp test is about 0.02 m/s for a high-elevation-angle satellite (when Selective Availability is off), the anomaly can be detected within 5 seconds as long as the maximum gradient amplitude is greater than 3.5 meters.

The next sensitivity case examines the "thickness" of the ionosphere spatial gradient, as shown in Figure 8. Again, the dark black line represents the baseline case (19 km). When the gradient thickness increases, the ramp becomes less steep, so the differential error is less severe. The maximum differential error is plotted as a function of ionosphere gradient thickness in Figure 9. The MQM Ramp test can detect the anomaly within 5 seconds as long as the gradient thickness is smaller than 35 km.

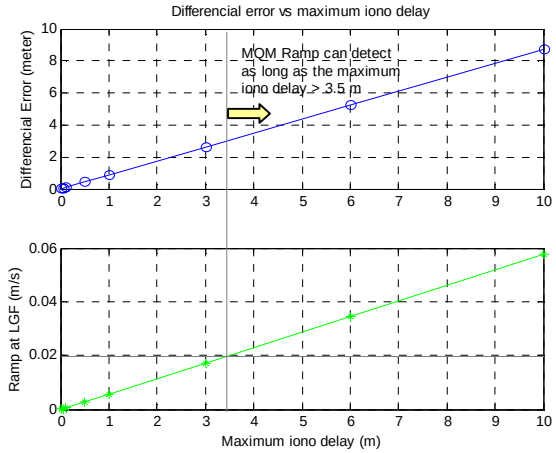

Figure 7: Maximum Differential Error vs. Ionosphere Gradient Amplitude

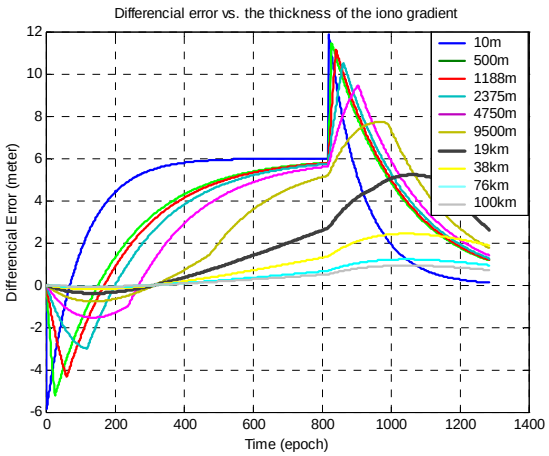

Figure 8: Differential Error Sensitivity to Ionosphere Gradient Thickness

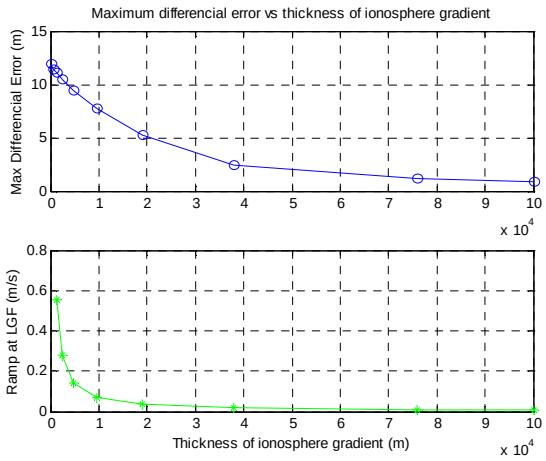

Figure 9: Maximum Differential Error vs. Ionosphere Gradient Thickness

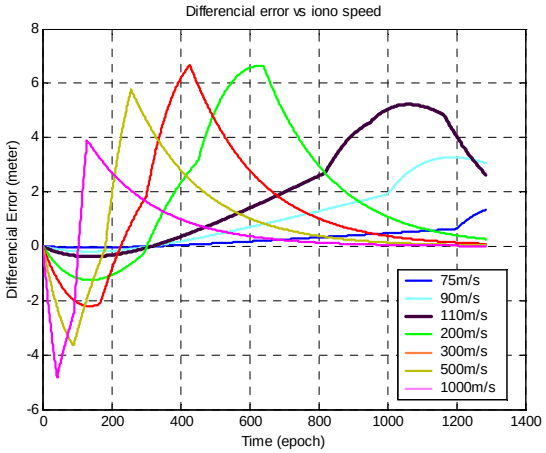

Figure 10: Differential Error Sensitivity to Ionosphere Gradient Speed

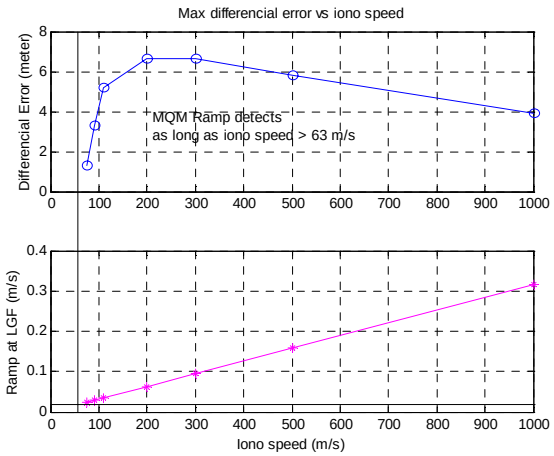

Figure 11: Maximum Differential Error vs. Ionosphere Gradient Speed

The results of varying the ionosphere wave front propagation speed are shown in Figure 10. The thick black line represents the baseline case (110 m/s) as before. When the wave front speed decreases, the actual induced range-domain ramp seen by the user becomes smaller; thus the differential error is reduced (note that if the front moves slower than 70 m/s, it cannot catch up with the aircraft in the "approach from behind" scenario modeled here). However, when the front moves too fast, the duration of the gradient is too short to significantly impact the ground and airborne smoothing filters. Thus, the maximum differential error peaks at a wave front speed of about 300 m/s, as shown in Figure 11

By comparing the ramp seen by the LGF with the MQM thresholds, we can show that the MQM will detect the anomaly within 5 seconds as long as the wave front speed is greater than 63 m/s. Since a front speed slower than 70 m/s will never “catch” the plane, MQM will rapidly detect

all ionosphere wave front anomalies that could affect an aircraft when the wave front approaches from behind.

We also exercised the simulation with different airplane approach speeds. The results are shown in Figure 12. As noted before, there will be no anomaly-induced differential error when the airplane is faster than the wave front. On the other hand, the slower the airplane flies, the longer time it is exposed to the wave front; thus it will suffer greater differential error. Since the LGF is not moving, it will always detect the anomaly regardless of the airplane approach speed.

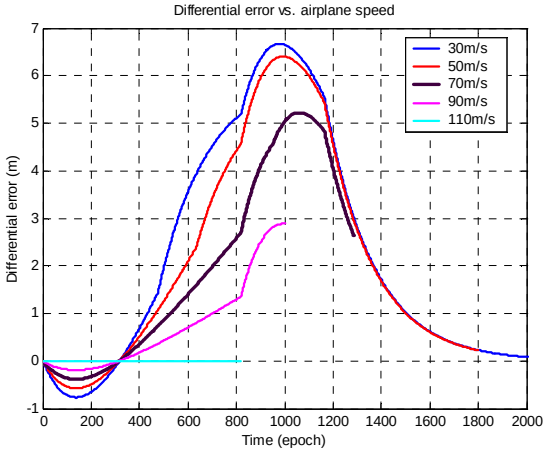

Figure 12: Differential Error Sensitivity to Aircraft Approach Speed

At the beginning of this paper, we crafted the near-worst-case scenario for a LAAS user. We assumed the airplane is approaching at the same direction as the ionosphere wave front. Given that an angle α exists between the two velocity vectors as shown in Figure 13, the resulting errors are plotted in Figure 14. Clearly the baseline case (thick black line) with $\alpha = 0$ is the worst.

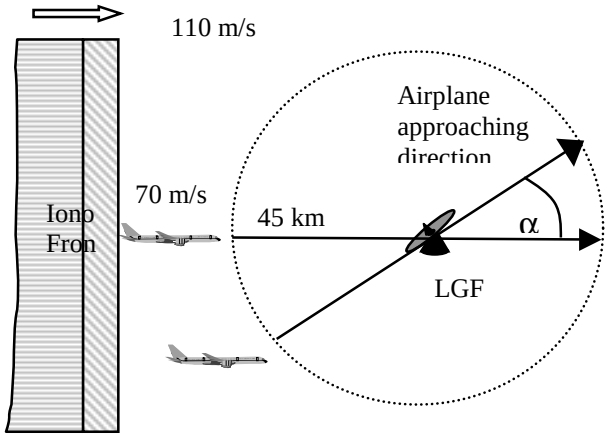

Figure 13: Top View of Airplane Approaching in a Different Direction than the Ionosphere Wave Front

Note that the differential error drops quickly as α diverges from zero. Even at ±30°, the maximum error is already reduced by 20-30%. This made clearer in the maximum error plot in Figure 15. When the angle is between 90° and 270°, the LGF is going to see the wave front first and flag the situation before the aircraft is impacted. This is another demonstrates of the importance of prompt LGF detection of ionosphere spatial anomalies.

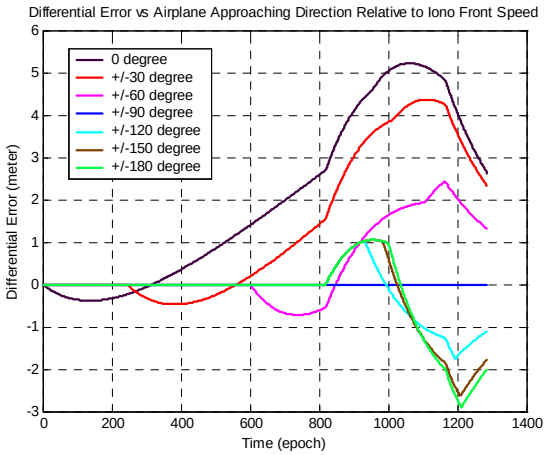

Figure 14: Differential Error Sensitivity to Angle between Aircraft and Wave Front Velocities

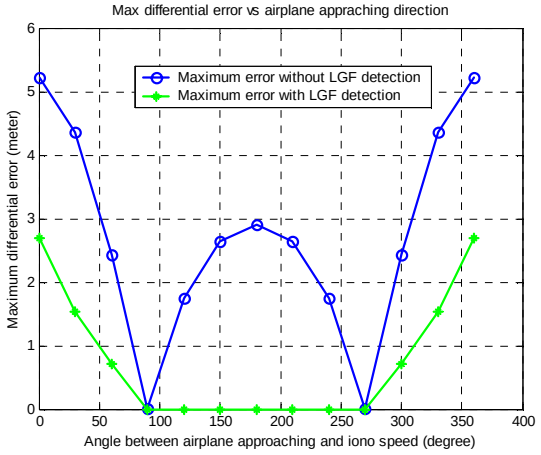

Figure 15: Maximum Differential Error vs. Angle between Aircraft and Wave Front

The variables included in the simulation, the ranges of variation, and the LGF ability of detection are all summarized in Table 2.

Parameter	Baseline value	Simulated variation	Comments
Max iono delay	6 m	0.01-10 m	MQM Step can detect it within 5 sec if the max iono delay > 3.5 m
Thickness of iono gradient	19 km	10 m-100 km	MQM Ramp can detect it within 5 sec seconds when the width < 35 km
Iono speed	110 m/s	75 – 1000 m/s	MQM Step can detect it within 5 seconds if the iono speed > 63 m/s
Airplane speed	70 m/s	30 – 110 m/s	MQM Step can always detect it within 5 seconds
Start distance of iono front and LGF	45 km	fixed	Farthest LAAS coverage
Angle between airplane approach and iono move	0	0 – 360 degree	No iono impact for 90 – 270 degree 0 degree is the worst case
Start distance between airplane and iono front	0	fixed	Maximize the exposure time of iono impact on differential error. 0 distance is the worst case
Satellite elevation	90	5 – 90 degree	Proportional to obliquity factor

Table 2: Summary of Model Parameters, Ranges Included in Simulation, and LGF Detection Ability

3.0 POSITION DOMAIN ANALYSIS

In order to translate range-domain results into user position errors, position-domain simulations were conducted using the Constellation ("Constell") Toolbox for Matlab to find the GPS satellite geometry at Washington D.C. for the 24-hour period (April 6-7, 2000) in which the ionospheric anomaly shown in Figure 1 was observed. For each set of satellite locations for a given GPS time during this period, the range-domain simulation is run for each SV in view according to its elevation angle, which is also used to calculate nominal range domain one-sigma errors (and the corresponding weighting matrix) based on the LAAS GAD C3 / AAD A error models [3]. Using the resulting weighted pseudo-inverse matrix, position-domain errors are computed.

Based on WAAS data, the ionosphere anomaly shown in Figure 1 was observed on April 6, 2000 at Washington D.C. at 21:32 (local time). There were nine satellites in view at that time. The sky plot at that time and location is shown in Figure 16. From the apparent ionosphere delay changes in the WAAS data, we assume that the wave front was approximately moving from North to South. As the front sweeps across the sky, the satellites are affected one after another. Recall that only the 19-km-thick ionosphere-gradient segment of the front would cause differential error within several minutes of the gradient crossing a user IPP. As soon as both the user and the LGF see the same ionosphere delay in carrier-smoothed code, there is no anomaly-induced differential error.

3.1 Fixed Satellite Geometry

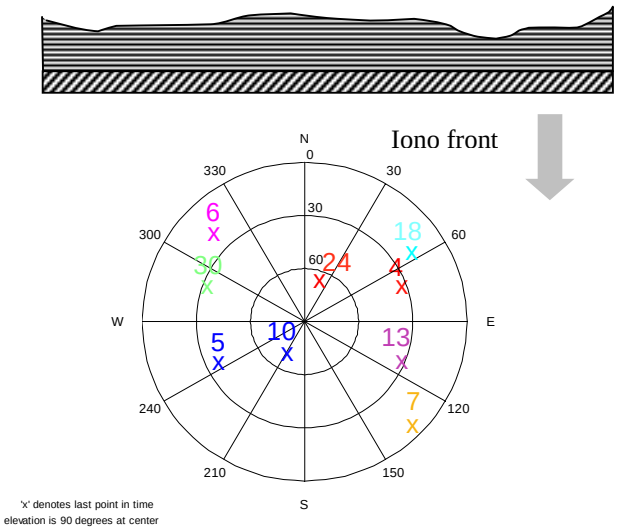

Figure 16: Sky Plot at Anomaly Time and Location, with Illustration of Ionosphere Wave Front

We will first consider the case where only one satellite is affected during an approach. It is not immediately clear if high-elevation or low elevation satellites will contribute more to position error. The lower the elevation angle, the greater the relative ionosphere error due to the higher obliquity factor [4]. On the other hand, the higher the elevation angle, the more weight that satellite will have in the position solution. The position errors during an airplane approach with different satellites affected are shown in Figure 17. PRN 24 is the "most sensitive" satellite for this geometry – if it is the satellite impacted, the maximum vertical position error is about 6.2 meters.

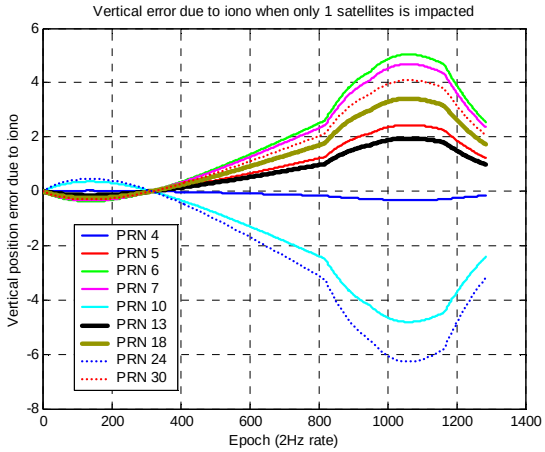

Figure 17: Vertical error with one Affected Satellite (Washington D.C., 20:30 on April 6, 2000)

If two (or more) satellites are close enough along one direction, it is possible that more than one satellite could be affected during one approach (about 10 minutes from VHF data broadcast reception to threshold crossing). Given a fixed North-to-South wave front direction, the maximum number of satellites that can be affected during one approach is two. Specifically, PRN 4 and PRN 24 can be both impacted (separated by 6 minutes) during one approach, as can PRN 10 and PRN 5 (separated by 3 minutes). Figure 18 shows the position domain error when both PRN 4 and 24 are affected. The resulting maximum vertical error is 2.7 meters. Similarly, the maximum vertical error is 3.4 meters when both PRN 10 and PRN 5 are affected.

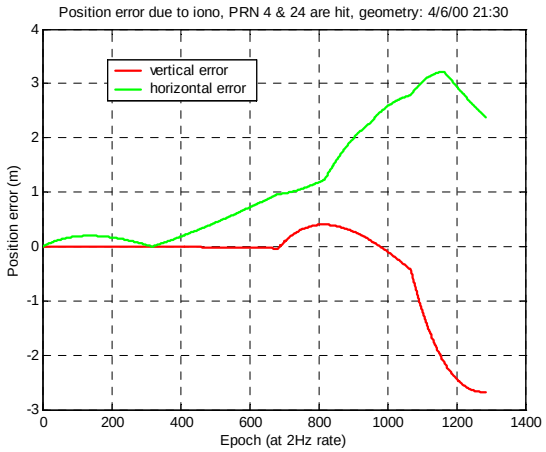

Figure 18: Position Error when PRN 4 and PRN 24 are Impacted During One Approach

Note that, in this particular case, the maximum vertical errors with two affected satellites are not as bad as the worst single satellite case (PRN 24) shown in Figure 17 because the two satellites were not hit by the ionosphere wave front simultaneously. Instead, one is hit several minutes after the other, and the effect of the second tends to cancel that of the first in its initial stages.

While the above two-satellite scenarios are likely to cover the vast majority of cases, we have also considered several "worst-case" scenarios. If the ionosphere wave front can move at any direction, then any two satellites could be affected simultaneously during one approach. In the scenario studied above, if we let the worst single satellite (PRN 24) combine with every other satellite in turn, the resulting position errors would be as shown in Figure 19. The worst single satellite case (PRN 24) is plotted with a thick black line for comparison. As before, almost all of these two-satellite cases have smaller vertical errors than the single-satellite PRN 24 case. The only exception is the combination of PRN 24 and PRN 10, where the maximum vertical error reaches 11 meters. If we let any pair of satellites be affected simultaneously (not necessarily including PRN 24), the results would be like the plot in Figure 20. The x-axis is the pair index number. Among all 36 combinations, the pair of PRN 24

and PRN 10 (index number 29) gives the worst maximum vertical error.

Figure 21 shows the result of an even worse case in which the anomaly wave front is curved to magically touch multiple (as many as all in view, in the extreme) satellites simultaneously. As we saw for the two-satellite case, more affected satellites do not generally lead to higher position errors. Among all combinations shown here, the worst vertical error is still that given by the two-satellite case (PRN 24 and PRN 10) identified in Figure 20.

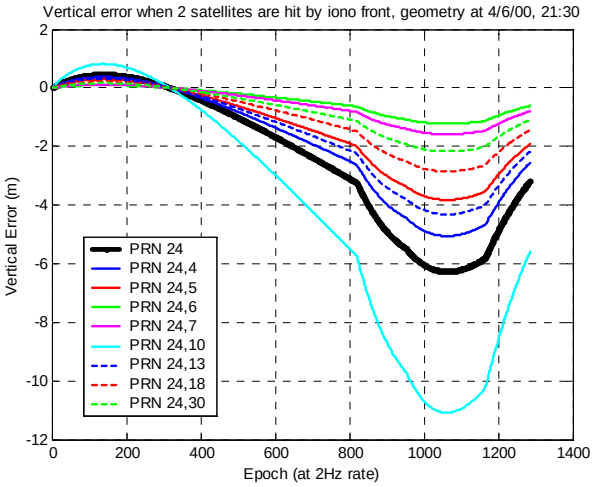

Figure 19: Two-Satellite Cases – PRN 24 Paired with Every Other Satellite in View.

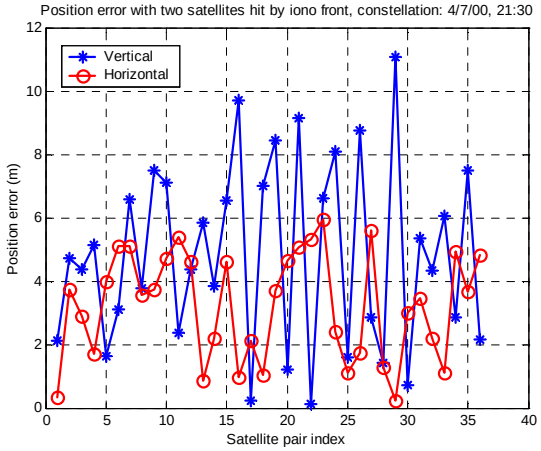

Figure 20: Two-Satellite Cases – Any Two Satellites are Paired Together

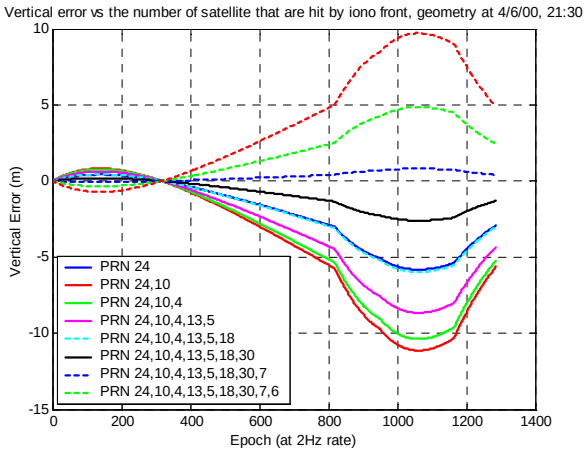

Figure 21: Multiple Affected Satellite Cases

3.2 "Multiple Worst Case" Over 24 Hours

Since the maximum position error strongly depends on the satellite geometry, we evaluated the ionosphere anomaly impact over the 24 hours following the observation of the anomaly on April 6, 2000 (after which the satellite geometries repeat). The time step used in the simulation is 10 minutes. As shown in Figure 22, the number of visible satellites at Washington D.C. (with a 5° mask angle) varied from 5 to 12 over this 24-hour period.

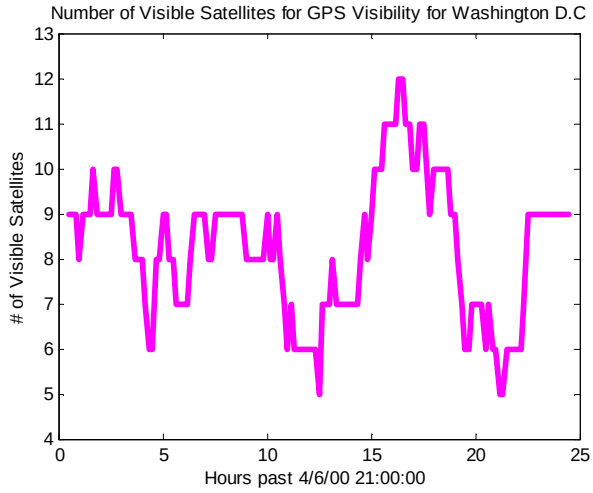

Figure 22: Number of Visible Satellites Over 24 Hours (Washington, D.C., April 6-7, 2000)

Assuming that only one satellite is affected by the baseline anomaly during a single approach, the worst position error (over all possible single-satellite cases) for each time step is shown in Figure 23. The maximum vertical error during 24 hours is about 18 meters. There are several occasions where the maximum vertical errors exceed 10 meters, which is significant because the Vertical Alert Limit (VAL) for Category I LAAS

precision approaches is 10 meters. When the vertical error is greater than VAL without annunciation, the situation is considered to be hazardous.

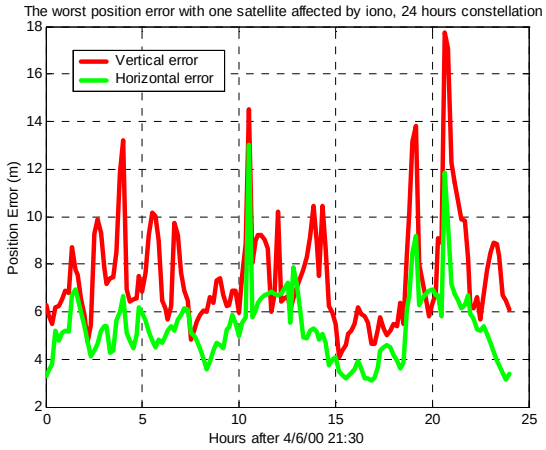

Figure 23: Maximum Position Errors Over 24 Hours (One Affected Satellite)

Assuming that two satellites are affected simultaneously during one approach, the worst position error at each time step is shown in Figure 24. Over all such cases, the maximum vertical error is 23 meters. The worst vertical errors exceed VAL at many epochs over 24 hour, although recall that only errors for the worst satellite pairs for each epoch are shown in the plot.

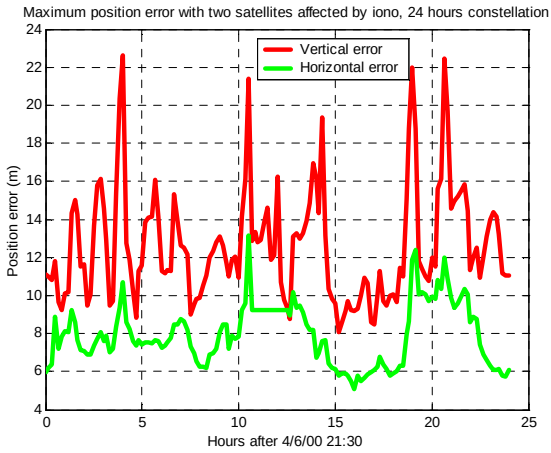

Figure 24: Maximum Position Errors Over 24 Hours (Two Affected Satellites)

While the worst-case results shown thus far in this section are worrisome, they only apply to a basic DGPS installation with no integrity monitoring. In Section 2.1, we demonstrated that LGF integrity monitoring would detect this type of ionosphere anomaly (and exclude the affected satellite(s)) promptly once the LGF IPP is impacted. This cuts short the growth of range-domain errors and thus reduces the worst-case position domain errors as well. The comparison with and without LGF detection is shown in Figures 25 and 26. The red lines on these plots are from Figures 23 and 24, while the cyan lines reflect range and position domain errors just after LGF impact (immediately before LGF detection and exclusion). LGF detection and exclusion has a significant effect: it reduces position errors by roughly a factor of 2, leaving only a small handful of worst-case scenarios where the 10-meter VAL is (just barely) exceeded.

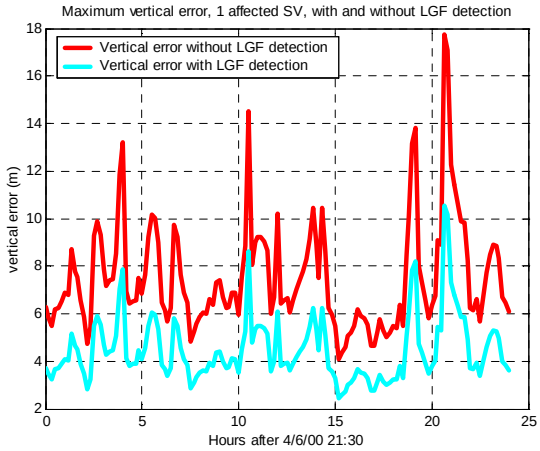

Figure 25: One-Satellite Cases With and Without LGF Detection

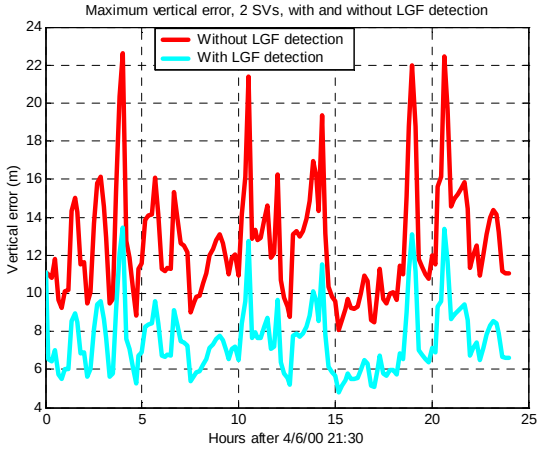

Figure 26: Two-Satellite Cases With and Without LGF Detection

3.3 Histograms of Vertical Position Errors

In the so-called "multiple worst case" scenarios as described in previous sections, i.e., when multiple parameters are all at their worst values, we have shown that vertical position errors can exceed the 10-meter VAL for Category I LAAS approaches. In order to put these extreme scenarios in perspective, it is instructive to

construct histograms of all scenarios simulated, not just the worst ones. Figure 27 shows histograms of the single--affected-satellite case under four conditions (from top to bottom): peak errors (worst-case anomaly impact time for a given approach) without LGF exclusion; peak errors with LGF exclusion; all errors (equal weighting to all impact times) without LGF exclusion; and all errors with LGF exclusion. These plots indicate that almost all simulated cases result in position errors below 10 meters.

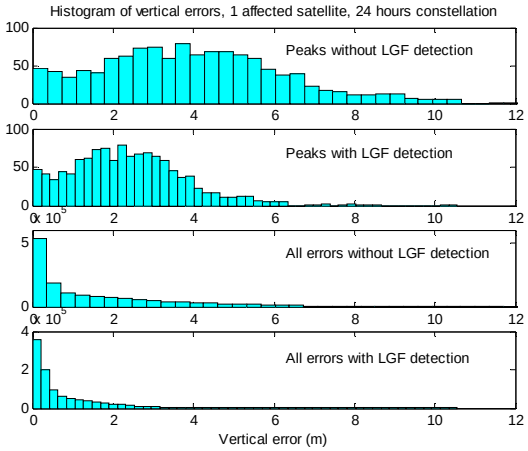

Figure 27: Histograms for One-Affected-Satellite Cases

To more clearly identify the probability of exceeding the 10-meter VAL, a semilog plot of one minus the Cumulative Distribution Function (CDF) is shown in Figure 28. Over the four cases defined above, the probability of a vertical error exceeding VAL, given that the ionosphere anomaly occurs and approaches from the worst direction ($\alpha = 0$), varies from about 0.05 (peaks only without LGF detection) to about 10^{-5} (all vertical errors with LGF detection).

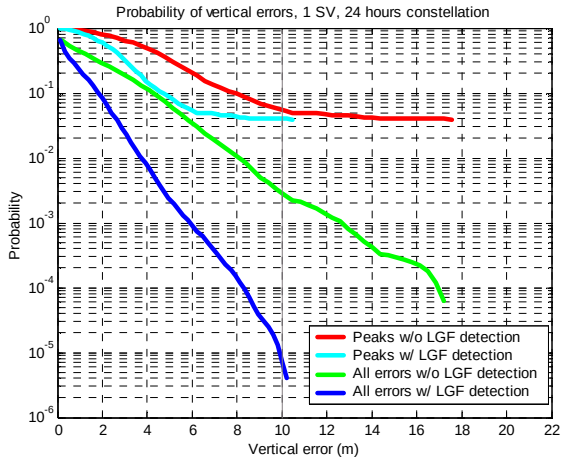

Figure 28: 1–CDF of Vertical Errors Over 24Hours (One Affected Satellite)

Similarly, histograms and probabilities for two-satellite cases are shown in Figures 29 and 30. The probability of vertical error exceeding VAL varies from about 0.1 (peaks only without LGF detection) to about 2×10^{-4} (all vertical errors with LGF detection).

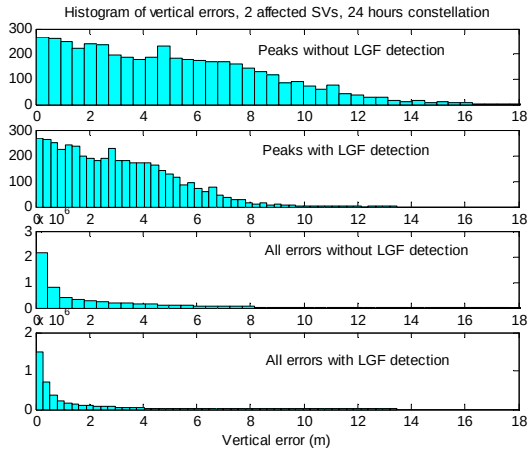

Figure 29: Histograms for Two-Affected-Satellite Cases

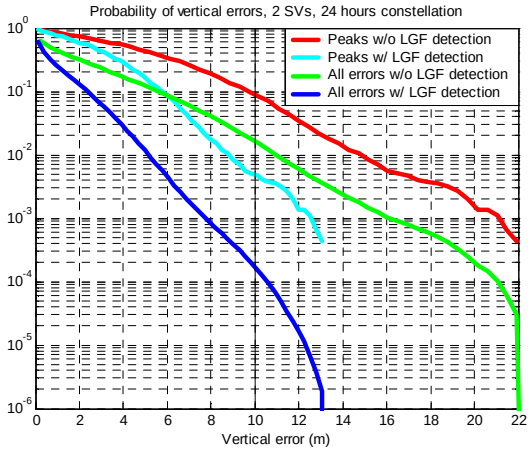

Figure 30: 1–CDF of Vertical Errors Over 24 Hours (Two Affected Satellites)

4.0 CONCLUSIONS AND MITIGATING STEPS

The impact of ionosphere spatial gradient anomalies (similar to those observed from WAAS supertruth data) on LAAS users has been evaluated. We found that, when multiple parameters describing the anomaly scenario are at their worst-case values, this anomaly could cause potentially hazardous vertical errors (greater than the 10-meter VAL) for aircraft conducting Category I precision approaches using LAAS. However, the probability of multiple conditions lining up to create such a hazard anomaly is very low. The anomaly must approach from almost directly behind an approaching aircraft, overtake

it, and time its impact on one or more satellite IPP's such that sufficiently large range errors occur before LGF detection and exclusion. Combining these probabilities together, as partially done in the histograms of Section 3.3, suggests that the likelihood of a hazardous error given that an anomaly of this type occurs is in the order of 10^{-4}. Thus, as long as the prior probability of the anomaly is 10^{-4} per approach or lower, the overall probability of a hazard is 10^{-8} per approach or less, which is small compared to the 2×10^{-7} LAAS Signal-in-Space Category I integrity risk requirement [9].

For Category I LAAS airports sited in zones of increased ionosphere activity (e.g., equatorial regions), it may be difficult to validate a 10^{-4} prior probability bound on ionosphere anomalies. In such locations, higher values of the broadcast ionosphere sigma (σ_{vig}) will be needed, and these values can be increased further when ionospheric storm activity occurs (this would have to be alerted by a separate system, such as WAAS) [8]. It is not possible to increase σ_{vig} enough to overbound the distribution of errors due to ionosphere anomalies, but it is possible to increase it enough to make the satellite geometries that lead to hazardous errors unavailable instead (so that users know that no LAAS approaches can be conducted). For the 24 hours of satellite geometries studied here, a typical value of σ_{vig} = 4 mm/km for CONUS provides 100% availability, as the computed nominal Vertical Protection Level (VPL_{H0}) is always less than the 10-meter VAL. However if σ_{vig} were increased by a factor of five to 20 mm/km, VPL_{H0} would exceed 10 meters for several epochs over 24 hours. These epochs correspond to the same epochs where the vertical error exceeds 10 meters (after LGF detection and exclusion) in Figures 25 and 26. As an example, the maximum vertical error with single affected satellite (same as in Figure 25 with LGF detection) was re-plotted in Figure 31 to compare with the calculated VPL_{H0} with increased σ_{vig}.

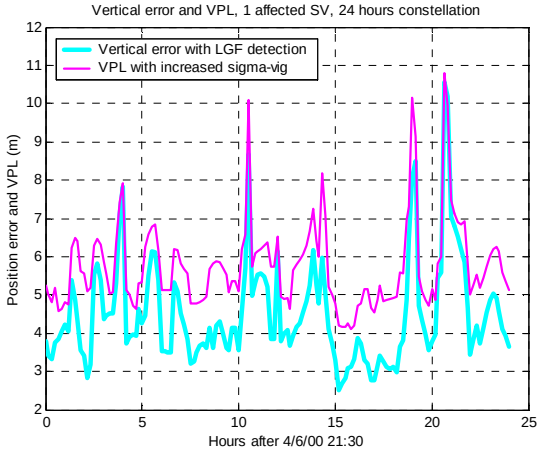

Figure 31: VPL_{H0} with increased σ_{vig} and the maximum vertical error with single affected satellite

A key factor in reducing the threat posed by ionosphere anomalies is early detection by the LGF. However, the LGF can only detect such anomalies once at least one LGF IPP is impacted. Thus, if further risk mitigation is needed (which is likely to be the case for Category II/III LAAS operations), means beyond simply enhancing LGF algorithms will be required. In addition to using multiple GPS frequencies (L1, L5, and perhaps L2) in future LAAS systems, two alternatives suggest themselves: (1) adding code-carrier divergence monitors to LAAS avionics and/or use aircraft inertial measurements account for aircraft motion so that LGF-style carrier-phase MQM can be conducted; and (2) adding reference receivers with longer baselines to LAAS-equipped airports so that the LGF observes ionosphere anomalies sooner. Both of these alternatives deserve further study to support Category II/III LAAS integrity requirements.

ACKNOWLEDGMENTS

The authors would like to thank the FAA LAAS Program Office (AND-710) for its support of this research. The opinions expressed here are those of the authors and do not necessarily represent those of the FAA or other affiliated agencies.

REFERENCES

[1] P. Misra, P. Enge, *Global Positioning System: Signals, Measurements, and Performance*. Ganga-Jamuna Press, 2001.

[2] S. Datta-Barua, *et.al.*, "Using WAAS Ionospheric Data to Estimate LAAS Short Baseline Gradients," *Proceedings of ION 2002 National Technical Meeting*. Anaheim, CA, January 28-30, 2002, pp. 523-530.

[3] *Minimum Operational Performance Standards for GPS/Local Area Augmentation System Airborne Equipment*. Washington, D.C., RTCA SC-159, WG-4A, DO-253A, Nov. 28, 2001.

[4] *Minimum Operational Performance Standards for GPS/Wide Area Augmentation System Airborne Equipment.* Washington, D.C., RTCA SC-159, WG-2, DO-229C, Nov. 28, 2001.

[5] *Specification: Performance Type One Local Area Augmentation System Ground Facility*. Washington, D.C., Federal Aviation Administration, FAA-E-2937A, April 17, 2002.

[6] G. Xie, *et.al.*, "Integrity Design and Updated Test Results for the Stanford LAAS Integrity Monitor Testbed (IMT)," *Proceedings of ION 2001 Annual Meeting*. Albuquerque, NM, June 11-13, 2001, pp. 681-693.

[7] B. Pervan, "A Review of LGF Code-Carrier Divergence Issues", Illinois Institute of Technology, MMAE Dept., May 29, 2001.

[8] S. Pullen, "Summary of Ionosphere Impact on PT 1 LAAS: Performance and Mitigation Options," Stanford University, Dept. of Aero/Astro, December 14, 2000.

[9] *Minimum Aviation System Performance Standards for Local Area Augmentation System (LAAS).* Washington, D.C., RTCA SC-159, WG-4A, DO-245, Sept. 28, 1998.